

# Dynamic Instability of Individual Microtubules Analyzed by Video Light Microscopy: Rate Constants and Transition Frequencies

R. A. Walker, E. T. O'Brien,\* N. K. Pryer, M. F. Sobeiro, W. A. Voter,\* H. P. Erickson,\* and E. D. Salmon

Department of Biology, University of North Carolina, Chapel Hill, North Carolina 27599-3280; and \*Department of Anatomy, Duke University, Durham, North Carolina 27710

**Abstract.** We have developed video microscopy methods to visualize the assembly and disassembly of individual microtubules at 33-ms intervals. Porcine brain tubulin, free of microtubule-associated proteins, was assembled onto axoneme fragments at 37°C, and the dynamic behavior of the plus and minus ends of microtubules was analyzed for tubulin concentrations between 7 and 15.5  $\mu\text{M}$ .

Elongation and rapid shortening were distinctly different phases. At each end, the elongation phase was characterized by a second order association and a substantial first order dissociation reaction. Association rate constants were 8.9 and 4.3  $\mu\text{M}^{-1} \text{s}^{-1}$  for the plus and minus ends, respectively; and the corresponding dissociation rate constants were 44 and 23  $\text{s}^{-1}$ . For both ends, the rate of tubulin dissociation equaled the rate of tubulin association at 5  $\mu\text{M}$ . The rate of rapid shortening was similar at the two ends (plus = 733  $\text{s}^{-1}$ ; minus = 915  $\text{s}^{-1}$ ), and did not vary with tubulin concentration.

Transitions between phases were abrupt and stochastic.

As the tubulin concentration was increased, catastrophe frequency decreased at both ends, and rescue frequency increased dramatically at the minus end. This resulted in fewer rapid shortening phases at higher tubulin concentrations for both ends and shorter rapid shortening phases at the minus end. At each concentration, the frequency of catastrophe was slightly greater at the plus end, and the frequency of rescue was greater at the minus end.

Our data demonstrate that microtubules assembled from pure tubulin undergo dynamic instability over a twofold range of tubulin concentrations, and that the dynamic instability of the plus and minus ends of microtubules can be significantly different. Our analysis indicates that this difference could produce treadmilling, and establishes general limits on the effectiveness of length redistribution as a measure of dynamic instability. Our results are consistent with the existence of a GTP cap during elongation, but are not consistent with existing GTP cap models.

**T**HE term "dynamic instability" describes microtubule assembly in which individual microtubules exhibit alternating phases of elongation and rapid shortening. Transitions between these phases are abrupt, stochastic, and infrequent in comparison to the rates of tubulin association and dissociation at the microtubule ends (17, 28). Substantial evidence has accumulated to indicate that dynamic instability is the basic mechanism of microtubule assembly in vitro (17, 28), and in both the mitotic spindle and the cytoplasmic microtubule complex (CMTC)<sup>1</sup> (10, 11, 34, 35, 37). Although microtubule dynamics within the cell may be regulated by various microtubule-associated proteins (MAPs) and other intracellular regulatory molecules, it is important

first to understand the details of the inherent behavior of microtubules assembled from tubulin alone.

The studies of Mitchison and Kirschner (28) and Horio and Hotani (17) provided strong evidence that dynamic instability was the mechanism of microtubule assembly and disassembly, but these studies were limited in their characterization of dynamic instability. Mitchison and Kirschner (28) used glutaraldehyde fixation of microtubules assembled from stable nucleation sites. This approach allowed the authors to analyze the behavior of microtubule populations over a range of tubulin concentrations. However, because microtubules were fixed at various time points, it was not possible to know the dynamic history of individual microtubules. Horio and Hotani (17) overcame this limitation by using dark-field microscopy to visualize the in vitro assembly of individual microtubules at video frame rates. While this approach directly demonstrated dynamic instability behavior for indi-

1. *Abbreviations used in this paper:* CMTC, cytoplasmic microtubule complex; DIC, differential interference contrast; MAP(s), microtubule-associated protein(s).

vidual microtubules, conclusions concerning the details of this behavior were also limited, since only one tubulin concentration was analyzed.

Complete characterization of microtubule assembly requires knowledge of the rate constants for tubulin association and dissociation during both the "elongation" and "rapid shortening" phases, the frequencies of transitions between these phases (we will use the term "catastrophe" for the transition from elongation to rapid shortening and "rescue" for the reverse transition), and the frequency of nucleation ("seeded nucleation" in our experimental system). This characterization requires: (a) visualization of individual microtubules over a range of tubulin concentrations; and (b) an imaging system that can acquire and resolve images at intervals much shorter than the duration of the shortest elongation or rapid shortening phase.

To achieve these requirements, we have used purified tubulin, seeded microtubule assembly, and video microscopy methods to visualize the dynamic behavior of individual microtubules. Seeded assembly allowed measurements to be made over an extended range of subunit concentrations, while the small number of seeds assured that the tubulin concentration remained essentially constant during an experiment. Using these methods, we were able to obtain independent measurements of the rate constants and transition frequencies for the plus and minus ends for tubulin concentrations between 7 and 15.5  $\mu\text{M}$ . These observations help to refine our understanding of the molecular events responsible for the dynamic behavior of microtubules.

## Materials and Methods

### Tubulin Purification

Previous studies of dynamic instability *in vitro* have used phosphocellulose-purified tubulin (17, 27, 28). This method, by itself, may not completely remove all associated proteins and may leave traces of enzymatic activity such as guanylate kinase (31, 40). To further purify our tubulin preparations, we have used a glutamate assembly cycle after phosphocellulose chromatography (40).

Porcine brain tubulin was purified by two cycles of assembly and disassembly in a buffer of 100 mM 2-(*N*-morpholino)ethane sulfonic acid (MES), 1 mM EGTA, 0.5 mM  $\text{MgSO}_4$ , 3.4 M glycerol, pH 6.6, followed by passage over phosphocellulose and a third cycle of assembly in 1 M  $\text{Na}^+$ -glutamate as described previously (40). The tubulin was then resuspended immediately in either PM buffer (100 mM Pipes, 2 mM EGTA, 1 mM  $\text{MgSO}_4$ , 1 mM GTP, pH 6.9) or in MES-glycerol buffer, and frozen in small aliquots. Tubulin stored in MES-glycerol buffer was transferred to PM buffer (no glycerol) before experiments.

We examined the purity of our tubulin preparations by both Coomassie Blue staining and silver staining (26, 30) of proteins separated on overloaded (50  $\mu\text{g}$  per lane) SDS-PAGE minigels. No high molecular weight proteins were visible in either preparation. To estimate the detection limits of the silver-staining method, we purified MAP 2 by the method of Voter and Erickson (39), and determined the minimum detectable load per lane on silver-stained gels. MAP 2 was undetectable at 0.3  $\mu\text{g}$  per lane. Based on this value, the percentage of MAP tubulin must be <0.6% in each tubulin preparation.

The fraction of active tubulin and the steady state free subunit concentration ( $S_{ss}$ ) for the tubulin preparations used in this study were determined by the methods of Mitchison and Kirschner (27). Briefly, aliquots of various concentrations of pure tubulin were assembled to steady state at 37°C, and then centrifuged (at 37°C) to pellet the assembled microtubules. The concentration of free tubulin was then plotted versus the concentration of total tubulin present in each sample. The concentration of soluble tubulin, extrapolated to zero total tubulin, was taken to be  $S_{ss}$ . The percentage of active tubulin in the three tubulin preparations used in this study ranged from 76 to nearly 100%, and  $S_{ss}$  ranged from 6.9 to 7.5  $\mu\text{M}$  (active tubulin).

Tubulin concentration values given in the text and figures reflect only active tubulin.

### Axoneme Preparation

Flagellar axoneme fragments were prepared from *Lytechinus pictus* according to the method of Bell et al. (2). Axonemes were osmotically demembrated and mechanically separated from sperm heads by homogenization in a solution of 20% sucrose in distilled water, using a handheld Dounce homogenizer (Kontes Glass Co., Vineland, NJ). Axonemes were resuspended and washed in isolation buffer composed of 0.1 mM NaCl, 4 mM  $\text{MgSO}_4$ , 1 mM EDTA, 7  $\mu\text{M}$   $\beta$ -mercaptoethanol, and 10 mM HEPES (pH 7.0). Dynein outer arms were removed by incubation in isolation buffer adjusted to 0.6 M NaCl for 30 min at 4°C. Residual sperm heads were found to enhance both nucleation and elongation, and were therefore removed by sedimentation of the axoneme preparation through an 80% sucrose cushion (16,000 g, 10 min). Axonemes were stored at -20°C in a 1:1 solution of isolation buffer/glycerol. Axonemes were washed and resuspended in PM before use.

### Assay of Microtubule Dynamics

Purified tubulin and axonemes were mixed and then diluted with cold PM to the desired tubulin concentration and held at 4°C. The axoneme ( $2.7 \times 10^7 \text{ ml}^{-1}$ ) and GTP (1 mM) concentrations were held constant for all preparations. A 5- $\mu\text{l}$  sample of the preparation was added to a clean slide, covered with a biologically clean (25) 22-mm<sup>2</sup> coverslip (thickness No. 0), and then sealed with valap (1:1:1 mixture of beeswax, lanolin, and petrolatum) to prevent drying and to prevent flow within the slide-coverslip chamber. The typical separation between inner glass surfaces was 10–20  $\mu\text{m}$ . The slide preparation was warmed to 37°C on the microscope stage to induce assembly. Stage temperature was maintained by a Sage model 279 or 279B air curtain incubator (Orion Research Inc., Cambridge, MA).

Although axonemes tightly adhered to the clean glass surfaces of the chamber, the microtubules assembled onto axonemes never adhered to either the coverslip or the slide. Free tubulin subunits also did not adhere to chamber surfaces, as demonstrated by two different methods. First, using fluorescently labeled tubulin (24, 43) and the fluorescent redistribution after photobleaching techniques of Wadsworth and Salmon (42), we found that >92% of free tubulin within the chamber was mobile. Second, microtubule elongation rates were similar in chambers of different surface-to-volume ratios.

Microtubules in the field of view did not appear to be affected by the illumination beam. Microtubule assembly in the slide-coverslip chamber was comparable (in terms of number and length) to preparations which were assembled in solution at 37°C and then placed on the microscope stage for observation. In addition, microtubule assembly in the field of illumination was similar to assembly in the unilluminated regions of the chamber.

We showed that the plus end was the faster elongating end in separate experiments by using the inherent morphological asymmetry (4) of *Chlamydomonas reinhardtii* axoneme fragments. However, sea urchin axoneme fragments were used routinely as nucleation seeds in this study because we were unable to reliably separate the *Chlamydomonas* axoneme fragments from debris that promoted and stabilized microtubule assembly. Microtubules assembled onto sea urchin axoneme fragments were identified as plus or minus ended based on rate of elongation.

We report data only for tubulin concentrations between 7 and 15.5  $\mu\text{M}$ . At tubulin subunit concentrations < 7  $\mu\text{M}$ , no microtubules were observed during 15–20-min searches of the slide-coverslip preparation after warming to 37°C. We were unable to analyze the kinetics of microtubule growth at tubulin concentrations >15.5  $\mu\text{M}$  because extensive self-nucleated microtubule assembly obscured the field of view, making analysis of individual, seeded microtubules impossible. In addition, extensive self-assembly of tubulin subunits into microtubules would have reduced the concentration of free tubulin subunits by an unknown amount.

### Video Microscopy

Microscopic methods were based upon those reported by Pryer et al. (33). Preparations were viewed by differential interference contrast (DIC) microscopy, using a Zeiss model 1 photomicroscope equipped with a Plan 100 $\times$ /1.25 NA oil immersion objective lens, DIC prisms, and a 1.4 NA condenser. An HBO 200 W mercury lamp (Osram, Berlin, Federal Republic of Germany) provided full illumination of the condenser aperture through heat-cut and 546-nm interference filters. Image magnification at the video camera faceplate was 350 $\times$ .

Image contrast was enhanced by analog and digital video processing (1, 18, 33, 36). Video image generation and analog contrast enhancement were provided by a video camera (model 67; Dage-MTI Inc., Michigan City, IN). Digital enhancement was provided by Max Video Image Processing boards (Datacube, Inc., Peabody, MA) housed in a computer (model CPU-ID Force, Inc., Los Gatos, CA). The image processor digitized live video into a  $512 \times 512$  pixel image with a 256 bit gray scale. An out-of-focus background image was averaged for 256 frames then stored in a frame buffer. This background image was subtracted from the live image and the result was fed into a real-time exponential average of two frames. Although increase in signal to noise is proportional to the square root of the number of frames averaged, we were limited to a two frame exponential average due to the rapid Brownian movement of microtubule ends in solution. Background subtraction and exponential averaging at video frame rates (33-ms intervals) required two arithmetic processor units in series, interconnected to three frame buffers.

Images were recorded on 3/4 inch U-matic tape through a Vicon model V240T or a Panasonic WJ-810 date-time generator into either a Sony model TVO-9000 or a Sony model VO-5800H videocassette recorder. Images recorded on the TVO-9000 were transferred onto 3/4 inch U-matic tape in the VO-5800H before analysis.

### Data Analysis

Microtubule elongation and rapid shortening rates were measured from videotape recordings played on a Sony VO-5800H. We developed a computer-based analysis system to follow microtubule length changes in real time. A point cursor, generated by an Apple II computer, was electronically overlaid on the video screen and used to track the end of the microtubule. Data points were taken by positioning the cursor with an Apple "mouse" and clicking the mouse button. Changes in microtubule length were plotted as a function of time, and the average rates of elongation and rapid shortening were determined by least squares regression analysis.

Based on repeated measurements of the position of the ends of individual microtubules at the same time point in the video records, the edge of the diffraction image of an elongating microtubule could be detected with an accuracy of  $<0.25 \mu\text{m}$ . However, this accuracy was limited in two ways. We could not measure microtubule elongation for microtubules  $<0.5 \mu\text{m}$ . It was difficult to detect the ends of these short microtubules due to the bright contrast generated by the axoneme. In addition, as a microtubule increased in length, the position of the end became more difficult to measure due to Brownian movement, particularly when microtubules were longer than  $20 \mu\text{m}$ . Due to the above limitations, the temporal resolution of our analysis system was estimated to be 0.5–1 s.

Photographs of the video monitor were taken on Kodak Panatomic-X film using a 0.5-s exposure to average 15 frames of running video and therefore reduce noise in the video image.

## Results

### Visualization of the Phases and Transitions Characteristic of Dynamic Instability

The dynamics of individual, seeded microtubules were clearly observed and recorded using our procedures for DIC microscopy, video contrast enhancement and digital image processing. This is illustrated in Fig. 1 for the assembly of microtubules at  $11.2 \mu\text{M}$  tubulin. Fig. 2 shows length changes of individual microtubules over a longer interval for the same axoneme shown in Fig. 1, and also demonstrates the phases and transitions characteristic of dynamic instability. Microtubules were observed to undergo dynamic instability at both ends at each tubulin concentration examined. In general, there were variable periods during which no microtubules were observed at the axoneme end. After nucleation from the axoneme seed, a microtubule elongated for a variable period of time before undergoing an abrupt transition (catastrophe) to rapid shortening. A microtubule in the rapid shortening phase either completely depolymerized back to the axoneme, or underwent an abrupt transition (rescue) back to the elongation phase.

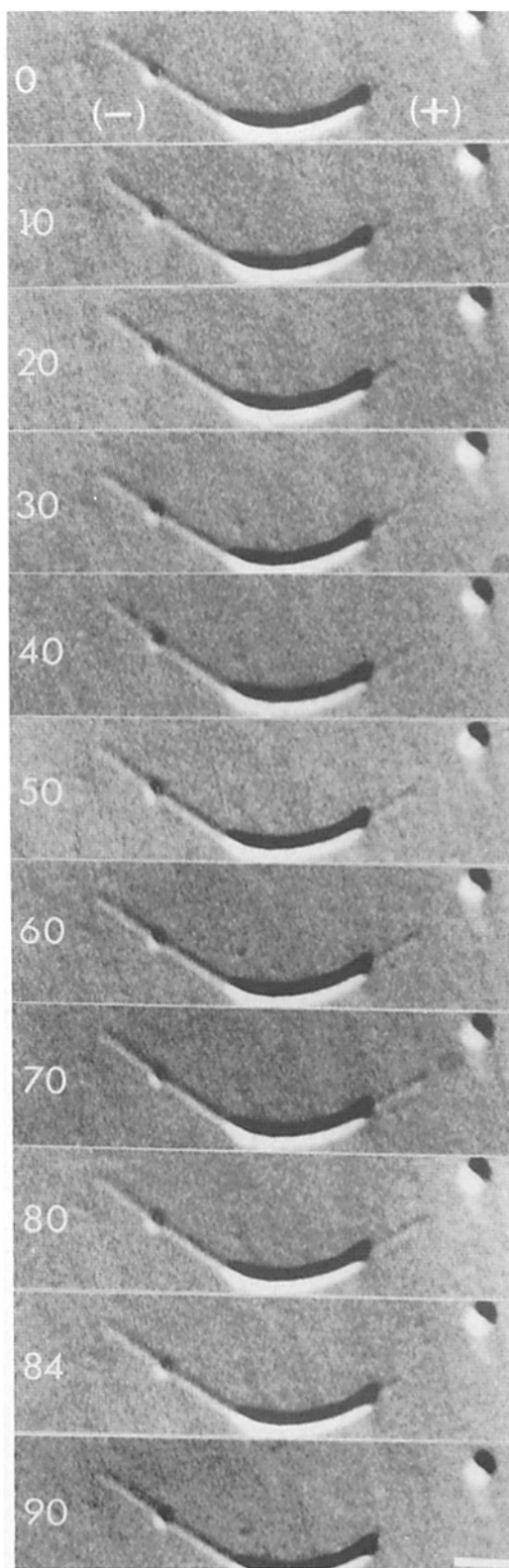


**Figure 1.** Video-enhanced contrast DIC images of dynamic instability behavior. The plus end microtubule was already in the elongation phase at 0 s and continued in the elongation phase for  $\sim 84$  s, then underwent a catastrophe and rapidly shortened to the axoneme end. The minus end slowly elongated over the same time period. Images were recorded  $\sim 20$  min after the preparation was warmed to  $37^\circ\text{C}$ . Tubulin concentration =  $11.2 \mu\text{M}$ . (All tubulin concentration values given in the figure legends and text reflect active tubulin concentration.) Bar,  $2 \mu\text{m}$ .

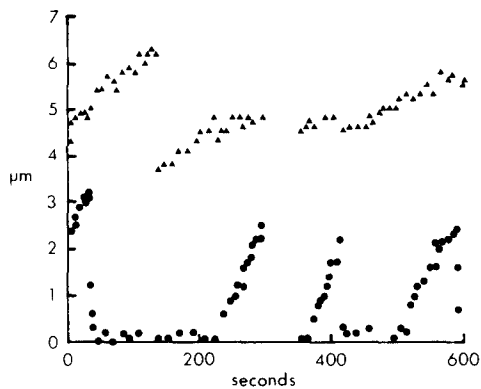


**Figure 2.** Changes in plus end and minus end microtubule length as a function of time. Four plus end microtubules (solid circles) and one minus end microtubule (solid triangles) exhibited dynamic instability behavior during the same time period. The minus end microtubule entered a pause period during which there was little change in length for  $\sim 3.5$  min. The last plus end elongation phase and subsequent rapid shortening phase plotted in this figure correspond to the sequence shown in Fig. 1.

At any given tubulin concentration in the range examined, the rates of microtubule elongation and of rapid shortening appeared constant throughout the duration of each phase of elongation and rapid shortening. However, in some rare cases ( $<1\%$ ), microtubules were observed to pause while in either the elongation or the rapid shortening phase. Pauses occurred at both microtubule ends, as shown for the plus end in Fig. 3, and for the minus end in Fig. 2. After a pause during elongation, a microtubule either rapidly shortened (Fig. 3 *a*), or resumed elongation (Figs. 2 and 3 *b*). The longest pause we observed is shown in Fig. 2. In this example, elongation of the minus end microtubule paused for  $\sim 3.5$  min during which the microtubule did not significantly change length. Pauses were more easily visualized during rapid shortening than elongation, because the greater rate of shortening provided a clearer contrast to the pause state. They were generally  $<5$  s (Fig. 3 *c*), and often were not measurable, appearing only as “glitches” as the microtubule depolymerized.

### Association and Dissociation Rate Constants

The average rates of elongation for plus and minus ended microtubules are plotted in Fig. 4 as a function of tubulin subunit concentration. We found that the rate of elongation was directly proportional to the free tubulin concentration for both ends, as deduced for tubulin preparations containing MAPs (3, 19) and for purified tubulin preparations (28). The rate of elongation of the plus end was about twice the rate of elongation of the minus end over the tubulin concentration range that we examined. In addition, we found a substantial dissociation rate during elongation.

Association and dissociation rate constants during elongation were calculated from the data in Fig. 4 (assuming 1,634 dimers/ $\mu\text{m}$ ). During the elongation phase, the rate of microtubule elongation,  $v^e$ , produced by end-dependent subunit association and dissociation reactions, is given for the two microtubule ends by:

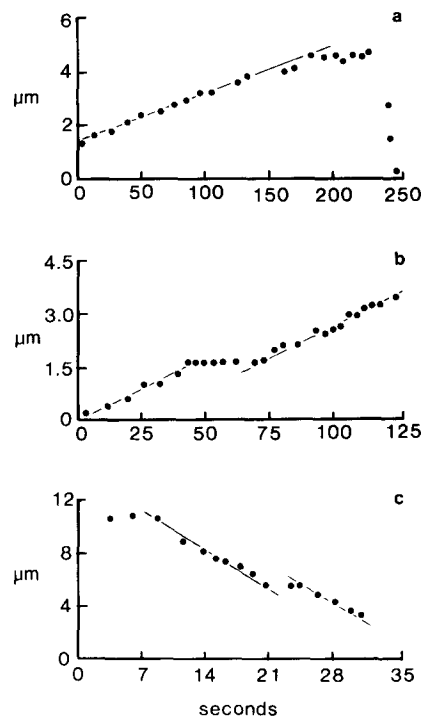


**Figure 3.** Pauses during microtubule elongation and rapid shortening. Change in microtubule length is plotted as a function of time. Solid lines represent average rates of elongation or rapid shortening as appropriate. Pauses could be seen as deviations from the average rate. (a) A plus end microtubule paused for 45 s then rapidly shortened to the axoneme. Tubulin concentration =  $8.8 \mu\text{M}$ . (b) A plus end microtubule paused for 30 s then resumed elongation. Tubulin concentration =  $9.8 \mu\text{M}$ . (c) A plus end microtubule paused for  $\sim 4$  s during rapid shortening. Tubulin concentration =  $9.8 \mu\text{M}$ . These sequences were specifically selected to show long duration pauses, but pauses were very rare events, occurring in  $<1\%$  of the phase durations analyzed.

$$v^{e+} = k_2^{e+}(s) - k_{-1}^{e+} \quad (1)$$

$$v^{e-} = k_2^{e-}(s) - k_{-1}^{e-}, \quad (2)$$

where  $(s)$  is the free tubulin subunit concentration,  $k_2^{e+}$  and  $k_2^{e-}$  are bimolecular association rate constants, and  $k_{-1}^{e+}$  and  $k_{-1}^{e-}$  are unimolecular dissociation rate constants. Values for  $k_2^{e+}$  and  $k_2^{e-}$  were determined from the slope of the linear regression lines through the plus and minus data sets, respectively. Values for  $k_{-1}^{e+}$  and  $k_{-1}^{e-}$  were determined from the rate axis intercepts of the extrapolated linear regression lines through the plus end and minus end data sets, respectively. Both the association and dissociation rate constants were about twofold greater at the plus end (Table I).

During the elongation phase, the tubulin concentration at which the rate of tubulin association is equal to the rate of dissociation is termed the critical concentration for elongation ( $S_c^e$ ). For each end,  $S_c^e$  is equal to the ratio  $k_{-1}^{e-}/k_2^{e-}$ , which is also the  $x$ -axis intercept of linear regression lines in Fig. 4. The values for the critical concentration of elongation for the two ends were very similar,  $\sim 5 \mu\text{M}$  (Table I).

The average rates of rapid shortening for the plus and minus ends are plotted as a function of tubulin concentration in Fig. 5. For each end, the rate of rapid shortening ( $v^{rs}$ ) was much greater than the rate of elongation. The association

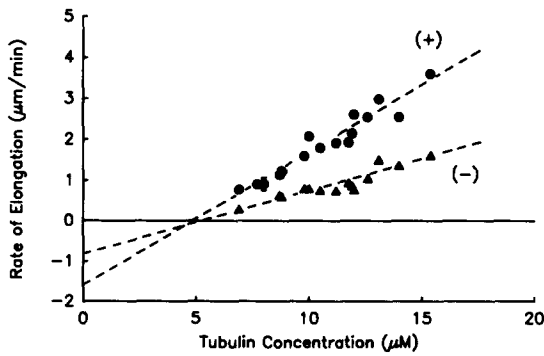


**Figure 4.** Rate of elongation as a function of tubulin subunit concentration (7–15.5  $\mu\text{M}$ ). Mean rate values for plus ends are indicated by solid circles. Mean rate values for minus ends are indicated by solid triangles. The slope (dashed lines) for each end was determined by linear regression analysis of the entire data set ( $n^+ = 391$ ;  $n^- = 260$ ) using Systat software (Evanston, IL). Error bars for the mean values correspond to SEM and were typically within the symbol size. This figure should not be confused with the nonlinear  $J_c$  plot for total microtubules reported by Carlier et al. (9). Their data reflects measurements of coexisting elongating and shortening microtubules, while our measurements and the extrapolations to the rate axis apply only to microtubules in the elongation phase.

and dissociation rate constants during rapid shortening can be calculated using Eqs. 1 and 2 (rate constants are denoted by “rs” instead of “e”). For each end, the rate of rapid shortening appeared to be independent of the free tubulin concentration. Therefore, the contribution of  $k_2^{\text{rs}}$  to the rate of rapid shortening was insignificant and  $k_{-1}^{\text{rs}}$  could be calculated directly from the rapid shortening rate. We determined  $v^{\text{rs}+}$  and  $v^{\text{rs}-}$  by averaging the entire plus and minus end data sets, respectively. The plus end shortened at  $\sim 27 \mu\text{m}/\text{min}$ , and the minus end shortened at  $\sim 34 \mu\text{m}/\text{min}$  ( $k_{-1}^{\text{rs}}$  values are given in Table I).

### Transition Frequencies: Seeded Nucleation, Catastrophe, and Rescue

The frequency of nucleation from an axoneme seed was stochastic and steeply concentration dependent. Seeded nucleation appeared to be more frequent at the plus end, as judged by the rate of elongation of the few microtubules present at the low tubulin concentrations. At 7.7  $\mu\text{M}$  tubulin, there was an average of 0.3 microtubules per axoneme, and no axoneme had microtubules at both ends. As shown in Fig. 6, at tubulin concentrations  $>10 \mu\text{M}$  most axonemes had microtubules at both ends, and, by 14  $\mu\text{M}$  tubulin, all axo-

**Table I.** Rate Constants for Association and Dissociation

Constants	Plus end	Minus end
Slope ( $\mu\text{m}/\mu\text{M min}$ )	$0.33 \pm 0.01$	$0.15 \pm 0.01$
$k_2^e$ ( $\mu\text{M}^{-1} \text{s}^{-1}$ )	$8.9 \pm 0.3$	$4.3 \pm 0.3$
x-intercept ( $\mu\text{M}$ )	$4.9 \pm 1.6$	$5.3 \pm 2.1$
y-intercept ( $\mu\text{m}/\text{min}$ )	$-1.59 \pm 0.50$	$-0.85 \pm 0.32$
$k_{-1}^e$ ( $\text{s}^{-1}$ )	$-44 \pm 14$	$-23 \pm 9$
$k_{-1}^{\text{rs}}$ ( $\text{s}^{-1}$ )	$733 \pm 23$	$915 \pm 72$

Slope, x-intercept, and y-intercept values were derived from the regression lines plotted in Fig. 4. Values for  $k_2^e$  and  $k_{-1}^e$  were determined as described in Results, and  $k_{-1}^{\text{rs}}$  values were determined by averaging the appropriate data set in Fig. 5. Values represent mean  $\pm$  SEM.

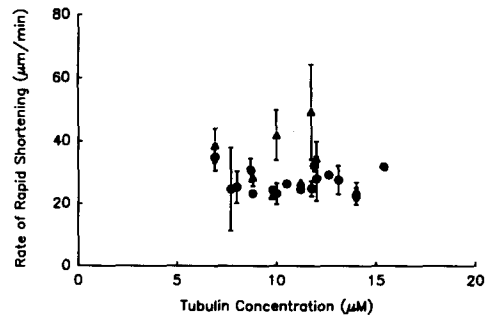


**Figure 5.** Rate of rapid shortening as a function of tubulin subunit concentration (7–15.5  $\mu\text{M}$ ). Mean rate values for plus ends are indicated by solid circles, and mean rate values for minus ends are indicated by triangles. Error bars correspond to SEM. The average rate of rapid shortening for each end was determined by averaging the entire data set of the appropriate end ( $n^+ = 104$ ;  $n^- = 41$ ).

nemes had microtubules present on both ends (5–6 microtubules per end).

Like seeded nucleation, both catastrophe and rescue appeared to be random events. There was no way to predict when a particular phase transition would take place, i.e., there was no indication that a microtubule elongated or shortened a particular distance or to a particular site on the microtubule before undergoing an abrupt transition. Further, at the tubulin concentrations where we were able to observe the entire duration of each elongation or rapid shortening phase, the duration of each phase varied considerably among different microtubules and for repeated phases involving the same microtubule. For example, the mean duration of plus end elongation at 7.7  $\mu\text{M}$  was  $2.6 \pm 1.3 \text{ min}$  ( $n = 7$ ), and the mean duration of minus end rapid shortening at 11.2  $\mu\text{M}$  was  $0.08 \pm 0.03 \text{ s}$  ( $n = 22$ ). In each case, the large standard deviation (relative to the mean) suggested a random process.

Since phase transitions appeared to occur independently of the duration already spent in a particular phase, we were able to obtain data from all elongation and rapid shortening phases, even if we could not observe each phase in its en-

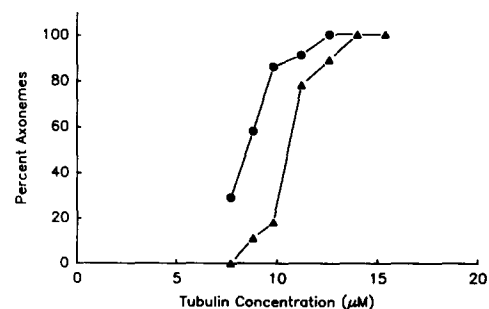


**Figure 6.** Seeded nucleation of plus and minus end microtubules as a function of tubulin concentration (7.7–15.5  $\mu\text{M}$ ). Microtubules were allowed to assemble for 15 min on the microscope stage before axonemes were observed. Solid circles indicate the percentage of axonemes at each concentration with microtubules on at least one end. Solid triangles indicate the percentage of axonemes at each concentration with microtubules on both ends. Microtubules which preferentially nucleated from the axoneme seed below 10  $\mu\text{M}$  were identified as plus end microtubules based on elongation rate. A total of 22–38 axonemes were scored at each concentration.

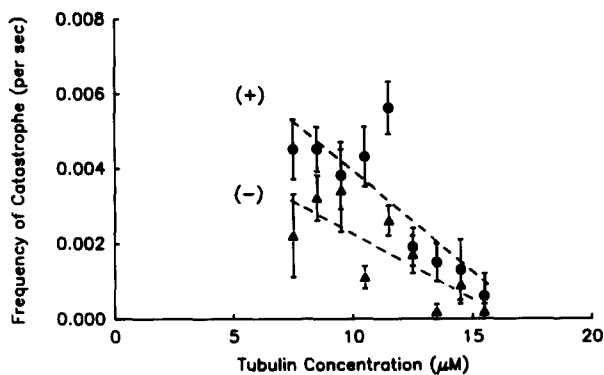


**Figure 7.** Frequency of catastrophe as a function of tubulin subunit concentration (7–16  $\mu\text{M}$ ). Solid circles indicate plus end data points, and solid triangles indicate minus end data points. Each point represents data from a 1  $\mu\text{M}$  concentration range (7–8, 8–9, etc.). The total time of elongation per data point was 35–282 min. Standard deviations were calculated as  $k_c/(\sqrt{n})$  (assuming a Poisson distribution), where  $n$  is the number of events counted (38). Linear regression lines are plotted through each data set.

tirety. We calculated the frequency of catastrophe ( $k_c$ ) for each tubulin concentration by (a) summing the time of elongation for all microtubules observed in elongation, and (b) dividing this time into the number of observed catastrophes. A similar method was used to calculate the frequency of rescue ( $k_r$ ).

Frequency of catastrophe is plotted as a function of tubulin concentration in Fig. 7. The frequency of catastrophe for each end decreased with increasing tubulin concentration, and the plus end catastrophe frequency appeared to be slightly greater over the concentration range studied.

Frequency of rescue is plotted as a function of tubulin concentration in Fig. 8. The minus end frequency of rescue increased significantly with increasing tubulin concentration, and, except for the lowest tubulin concentration, was significantly greater than the frequency of rescue at the plus end. The frequency of rescue at the plus end was less sensitive to tubulin concentration.

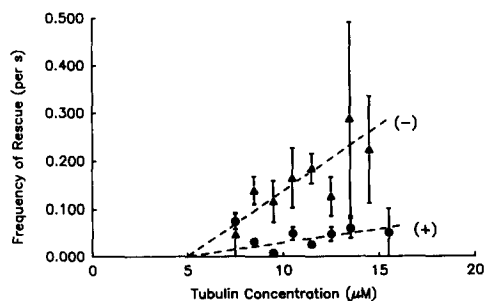


**Figure 8.** Frequency of rescue as a function of tubulin subunit concentration (7–16  $\mu\text{M}$ ). Solid circles indicate plus end data points, and solid triangles indicate minus end data points. Each point represents data from a 1  $\mu\text{M}$  concentration range (7–8, 8–9, etc.). The total time of rapid shortening per data point was 0.12–8.8 min. Standard deviations were calculated as described in Fig. 7, except that  $k_r$  replaced  $k_c$ . The linear regression lines through each data set were calculated assuming that the lines intercepted the x-axis at 5  $\mu\text{M}$  tubulin as described in the Discussion.

## Differential Dynamic Instability between Opposite Microtubule Ends

There was a noticeable difference in the mass of microtubule polymer assembled from the plus and minus ends of axoneme fragments over long periods of assembly at 10–11  $\mu\text{M}$  tubulin. During the initial 1–10 min of assembly, there was usually more polymer at the plus ends of axonemes because seeded nucleation was more frequent and the rate of elongation was faster at the plus ends. However, by 45 min there was usually much more polymer at the minus ends of the axonemes. At 10–11  $\mu\text{M}$  tubulin, plus end microtubules were rarely rescued before complete depolymerization took place. In contrast, the rapid shortening of minus ended microtubules was almost always rescued. Once nucleated from an axoneme seed, a minus ended microtubule persisted and steadily increased in length through repeated cycles of elongation and rapid shortening.

## Discussion

Our observations of individual microtubules confirmed that microtubules alternate between an elongation phase and a rapid shortening phase. Transitions between phases were abrupt, stochastic, and occurred very infrequently compared with the frequency of tubulin association and dissociation events. By combining high temporal resolution of individual microtubules with seeded assembly of extremely pure tubulin, we have also obtained new information concerning the details of dynamic instability behavior. We found that: (a) the rate of elongation during the elongation phase was proportional to tubulin concentration; (b) the plus end association rate constant for elongation was twofold greater than the minus end value; (c) plus and minus end microtubules exhibited significant dissociation rates during elongation; (d) there was little difference between the critical concentrations for elongation at the plus and minus ends; (e) the rate of rapid shortening was similar for the two ends and appeared independent of tubulin concentration; (f) microtubules occasionally paused during both elongation and rapid shortening; (g) seeded nucleation was more frequent at the plus end, and, for both ends, was a sensitive function of tubulin concentration; (h) higher concentrations of tubulin reduced the frequency of catastrophe at both ends and increased the frequency of rescue at the minus end; (i) the frequency of catastrophe was slightly greater at the plus end; and (j) the frequency of rescue was greater at the minus end.

## Microtubule Elongation and Rapid Shortening Occur by Independent Mechanisms

With few exceptions, the rate of elongation and the rate of rapid shortening at a particular tubulin concentration occurred at a constant rate. Furthermore, the rate of elongation was directly proportional to the tubulin concentration. These findings are consistent with association and dissociation of single tubulin subunits at the ends of microtubules.

The association rate constant values determined in this study ( $k_2^{e+} = 8.9 \mu\text{M}^{-1} \text{s}^{-1}$ ,  $k_2^{e-} = 4.3 \mu\text{M}^{-1} \text{s}^{-1}$ ) were significantly greater than those reported in previous studies using phosphocellulose purified tubulin (Mitchison and Kirschner [28]:  $k_2^{e+} = 3.82 \mu\text{M}^{-1} \text{s}^{-1}$ ,  $k_2^{e-} = 1.22 \mu\text{M}^{-1} \text{s}^{-1}$ ; Gard and Kirschner [15]:  $k_2^{e+} = 1.4 \mu\text{M}^{-1} \text{s}^{-1}$ ). These ear-

lier studies determined rate constants by a population assay, i.e., the net growth rate was measured by dividing the mean length of a population of microtubules by the incubation time between initiation of assembly and glutaraldehyde fixation. This method can greatly underestimate the rate of elongation during the elongation phase, since estimates of net growth will be reduced by any lag in nucleation from the seed and/or by catastrophes that occur during the incubation time. Even using video microscopy, one will underestimate rates (and transition frequencies) if images are not acquired and resolved much faster than the shortest period of elongation or rapid shortening.

Neglecting the effects of dynamic instability could also produce incorrect conclusions about the mechanism by which MAPs affect microtubule assembly. For example, Gard and Kirschner (15), using a population assay, report an apparent  $k_2^{e+}$  of  $1.4 \mu\text{M}^{-1} \text{s}^{-1}$ . Addition of XMAP, a protein purified from activated *Xenopus* eggs, appeared to stimulate a 10-fold increase in the rate of microtubule assembly at the plus end. They concluded that XMAP promoted polymer formation by increasing the association rate constant for tubulin elongation 10-fold. However, when compared with our value for the plus end association rate constant for pure tubulin, XMAP appears to increase  $k_2^{e+}$  only slightly (less than twofold: from  $8.9 \mu\text{M}^{-1} \text{s}^{-1}$  to  $15 \mu\text{M}^{-1} \text{s}^{-1}$ ). Rather than simply increasing the association rate constant during elongation, it is possible that XMAP increased the apparent rate of microtubule assembly primarily by one or more of the following: promotion of seeded nucleation, inhibition of catastrophe, and/or promotion of rescue.

We also found that the dissociation rates during elongation at the plus ( $44 \text{s}^{-1}$ ) and minus ( $23 \text{s}^{-1}$ ) ends were significantly faster than the values reported by Mitchison and Kirschner (28) ( $k_{-1}^{e+} = 0.37 \text{s}^{-1}$ ;  $k_{-1}^{e-} = 1.1 \text{s}^{-1}$ ). The origin of this difference between our results and those of Mitchison and Kirschner is unclear. It may be due to differences in the methods used to measure the rate of elongation as discussed above, or to effects of undetected MAPs in their tubulin preparation (23).

The kinetic events during the rapid shortening phase were best described by a first order dissociation rate constant. As shown in Fig. 5, the rate of rapid shortening did not decrease at higher tubulin concentrations, which indicates that there is no significant tubulin association during the rapid shortening phase.

At all tubulin concentrations analyzed, the rapid shortening phase was different from the elongation phase in several respects. For both ends of a microtubule, the rate of tubulin dissociation during rapid shortening ( $k_{-1}^{rs}$ ) was much greater than the dissociation rate during elongation ( $k_{-1}^e$ ). This result is in agreement with observations from bulk polymerization experiments (9) and measurements of average microtubule length changes over time (28). The rates of rapid shortening at both the plus and the minus ends were similar ( $k_{-1}^{rs+} = 733 \text{s}^{-1}$ ;  $k_{-1}^{rs-} = 915 \text{s}^{-1}$ ). This is in contrast to the twofold difference in association and dissociation rates between ends during the elongation phase.

### Pauses Occur Infrequently

Pauses were occasionally detectable during both elongation and rapid shortening phases. Their duration was highly variable, from a few seconds to several minutes. Pauses may have

occurred more frequently than we could detect, given the temporal and spatial resolution of our image acquisition system. The molecular origin of pauses is unknown, and pauses during elongation may be different from pauses during rapid shortening. Pauses may be the result of the nonproductive binding of tubulin subunits (6, 48), the insertion of a defective tubulin dimer into the microtubule lattice, or some other presently unknown mechanism. On the other hand, pauses may represent a naturally occurring intermediate state between elongation and rapid shortening.

### GTP Cap

The molecular basis of dynamic instability is thought to be some form of cap that stabilizes the end of an elongating microtubule (reviewed by Kirschner and Mitchison [21]). The favored model is the "GTP cap" as proposed by Mitchison and Kirschner (28) and based on earlier ideas that GTP hydrolysis and microtubule assembly might not occur simultaneously (7, 20, 32). It has been well established that GTP-tubulin adds to the end of an elongating microtubule and that the GTP is subsequently hydrolyzed (7, 13, 22, 46). The GTP cap model postulates that this hydrolysis produces a labile core of GDP-tubulin within the microtubule, which is capped at the elongating end by a more stable region of GTP-tubulin subunits. Catastrophe is the loss of the GTP cap, and rescue is the recapping of a GDP-tubulin end during rapid shortening.

Most proposed models explaining how the GTP cap is maintained and lost picture the cap as a dynamic structure, changing in size as GTP-tubulin subunits are continuously added and removed. In previous models, only two reactions were thought to contribute significantly to cap dynamics. Subunits were added to the cap as GTP-tubulin polymerized onto the microtubule end, and were lost from the cap as the bound GTP was hydrolyzed. A third possible mechanism, dissociation of GTP-tubulin from the cap, was not considered to contribute to cap dynamics, primarily because of results indicating that dissociation during the elongation phase (presumably of GTP-tubulin subunits) was negligible (28).

Models based solely on the first two reactions (association and hydrolysis) are, however, difficult to reconcile with our observations. First, we found that the frequency of catastrophe is not steeply dependent on elongation rate: it decreases only two- to threefold from 7 to  $15.5 \mu\text{M}$  free tubulin, i.e., from near steady state to twofold higher. This means that the cap must remain small enough to permit an appreciable frequency of catastrophe over this concentration range. Second, the frequency of catastrophe is similar at the two ends, even though the plus end elongates twice as fast as the minus end. This strongly suggests that the mechanisms for limiting cap size and generating catastrophe must have some features that are independent of microtubule polarity and elongation rate. In light of these new constraints, we are now able to critically evaluate existing GTP cap models.

The "stochastic hydrolysis" model for the GTP cap (7, 28), in which subunits are lost from the cap by a first order hydrolysis reaction subsequent to their association, predicts a very steep dependence of catastrophe on elongation rate. For example, a twofold change in elongation rate would change the catastrophe frequency by a factor of 10–100 (41). This model would also predict a 10- to 100-fold difference in

catastrophe frequencies at the two ends, since they differ in elongation rate by a factor of two. The simple stochastic hydrolysis model is thus incompatible with our observations on both points.

The “directed elongation” or “interface hydrolysis” model (5, 6, 8, 9) postulates hydrolysis at a fixed rate at the interface between cap and core. In this case, catastrophe should be observed only over an extremely narrow concentration range, presumably near steady state. At lower tubulin concentrations, where hydrolysis exceeds elongation, no cap would have a chance to grow. At higher concentrations, whenever elongation exceeds the fixed hydrolysis rate, the cap should grow indefinitely, essentially eliminating the possibility of catastrophe. This type of model is inconsistent with our observation that catastrophes still occur at tubulin concentrations twofold higher than steady state.

The model of Chen and Hill (12) is perhaps the most complete formal description of cap dynamics. It includes association and dissociation of subunits from five growing points, and up to 24 variations in hydrolysis rate, depending on the presence and state (GTP or GDP) of neighboring subunits. This model can easily fit our catastrophe data for a single end, using only two variations in hydrolysis rate (specifically, accelerated hydrolysis for the DD and DT neighbor configurations, which was the key feature proposed by Hill and Chen [16]). The problem is that accelerated hydrolysis must be polar, and if postulated at the plus end, it will eliminate the cap at the other end (at the minus end the interface between core and cap will always have the DT configuration, and accelerated hydrolysis would eliminate the entire cap). One could perhaps find some combination of the 24 possible hydrolysis rates that would give similar catastrophe frequencies at the two ends, but we have not yet found a scheme that is simple enough to be credible.

Each of these GTP cap models has focused on hydrolysis as the primary mechanism for loss of subunits from the cap, and they have differed mainly in their proposals for the rate and location of hydrolysis. However, our data indicate that a second mechanism significantly contributes to cap loss. Dissociation of GTP-tubulin subunits during elongation was not considered important in the above models, since Mitchison and Kirschner (28) reported a dissociation rate ( $0.37 \text{ s}^{-1}$ ) that was  $<1\%$  of the association rate ( $53 \text{ s}^{-1}$  at their  $14 \mu\text{M}$  steady state). In contrast, we have found that the rate of dissociation events ( $44 \text{ s}^{-1}$  for the plus end) is about half the rate of association events ( $89 \text{ s}^{-1}$  at  $10 \mu\text{M}$ ), and we therefore conclude that dissociation of GTP subunits makes a major contribution to the dynamics of the cap.

As discussed above, two of our observations suggest that a mechanism must exist to limit the size of the cap. This implies some sort of forced, coupled, or accelerated hydrolysis at each microtubule end. As pointed out previously (31), a simple mechanism that allows forced hydrolysis while maintaining a cap at microtubule ends is a “one subunit deep” cap model. This model envisions hydrolysis being forced only when a subunit becomes buried in the polymer lattice. In the simplest version of this model (e.g., for a linear polymer), the cap would consist of only a single subunit, loss of which would result in catastrophe. If microtubules behaved like a linear polymer with a single subunit cap, the frequency of catastrophe would be independent of tubulin concentration;

a prediction clearly contradicted by our data. Since, however, the microtubule wall is a helical, two-dimensional polymer, one can extend this model of hydrolysis to allow a larger cap. If hydrolysis occurs only when a GTP-tubulin subunit becomes buried in the polymer, a GTP cap could have up to one subunit per protofilament, or a maximum of 13 subunits. The actual number, and the overall complexity of the cap, depends on the number of growing points per microtubule end (e.g., 1, 3, 5, 13), and which particular subunit-subunit bond triggers hydrolysis. If catastrophe for the entire microtubule end is prevented by the presence of a single GTP-tubulin subunit, the remaining GTP-tubulin subunits would be free to dissociate without inducing rapid shortening.

This “stochastic dissociation, coupled hydrolysis” model thus provides a mechanism to limit the maximum size of the cap to the same small size at both microtubule ends, while also allowing for significant dissociation from each end without immediate cap loss. The model pictures the balance of stochastic association and dissociation events as the primary factor in determining the frequency of cap loss, while coupled hydrolysis provides the mechanism necessary to maintain an appreciable frequency of catastrophe at high rates of elongation. Using this model, we can explain one of our key observations that posed problems for earlier models: that the frequency of cap loss at opposite microtubule ends, having a two- to threefold difference in elongation rate, is very similar. This explanation is based on our experimental observation that the critical concentration during elongation (Table I) is essentially equal at the two ends. Since this critical concentration represents the balance of association and dissociation of GTP-tubulin subunits onto and from the cap, the equality requires that cap loss be approximately the same at the two ends. Finally, limiting the cap size to 13 subunits is also consistent with recent observations of very rapid cap loss after dilution (Voter, W.A., and H. P. Erickson, manuscript in preparation). In these experiments, disassembly began immediately (within 1 s) from both microtubule ends after a 15-fold dilution, consistent with a cap size shorter than 20–40 subunits.

We have done computer simulations for a number of stochastic dissociation, coupled hydrolysis models, and so far the most attractive is one that envisions one growing point per microtubule end. In this case, the cap could vary from 1 to 13 GTP-tubulin subunits per microtubule end, depending on the relative rates of subunit addition and dissociation for a particular subunit concentration. Addition of a 14th subunit would force or accelerate hydrolysis of the GTP on the now buried subunit. At the same time, a maximum of 12 GTP-tubulin subunits at the end are free to dissociate without inducing catastrophe. Simulations of cap dynamics using this model, and incorporating our experimentally derived rate constants for association and dissociation, correctly predicted the frequency of catastrophe at  $10 \mu\text{M}$  tubulin. However, the concentration dependence of the frequency of catastrophe, on either side of  $10 \mu\text{M}$ , was significantly steeper than our observed values. We must conclude that there are additional mechanisms, not yet appreciated, that operate to reduce the concentration dependence of catastrophe. So far we have limited our modeling to the incorporation of our experimental values for association and dissociation, and the single speculative parameter of coupled hydrolysis. We are



hopeful that an expanded model, perhaps incorporating one or more addition mechanisms, will provide a complete description of cap dynamics, and thus of dynamic instability.

An alternative explanation for the dynamic instability behavior of microtubules is the preferential binding of a MAP to the elongating end of a microtubule. A MAP may provide a capping function by itself (a “MAP cap”), or it may interact with the inherent tubulin capping mechanism to modify microtubule dynamics. We do not think that we were measuring the dynamics of a MAP-modified cap for two reasons. First, our tubulin preparations were extremely pure. No associated proteins were detectable on heavily loaded gels. Second, we have preliminary evidence from fluorescent redistribution after photobleaching that brain MAPs bind quickly and tightly to the glass surfaces of the slide-coverslip chamber (Pryer, N. K., R. A. Walker, M. F. Soboeiro, and E. D. Salmon, manuscript in preparation). If any residual MAPs were present in our tubulin preparations, the glass surfaces would effectively remove them from solution.

### Seeded Nucleation

We observed that frequency of nucleation from axoneme fragments was extremely sensitive to tubulin concentration (Fig. 6). This sensitivity suggests that seeded nucleation is a cooperative process. Seeded nucleation could involve either the formation and binding of an oligomer of tubulin, or the simultaneous binding of tubulin subunits to multiple sites at the ends of an axoneme. Since subunits at the broken ends of an axoneme are probably GDP-tubulin (47), seeded nucleation may be governed by the stochastic aspects of capping an axoneme end with sufficient numbers of GTP-tubulin subunits to sustain elongation.

### Rescue

In principle, rescue can not occur for tubulin concentrations less than the critical concentration for elongation,  $S_c^e$ . We found that  $S_c^e$  is  $\sim 5 \mu\text{M}$  for both ends (Fig. 4). At concentrations below  $S_c^e$ , there is no elongation and thus no observable rescues are expected. The linear regression lines through the data in Fig. 8 were calculated assuming that rescue must be zero at  $5 \mu\text{M}$  tubulin. The minus end data in Fig. 8 increases with tubulin concentration above  $5 \mu\text{M}$ . The concentration dependence of the plus end data above  $5 \mu\text{M}$  is less certain. However, it is clear that frequency of rescue at the minus end is much greater than occurs at the plus end at the higher tubulin concentrations.

The apparent linear dependence of rescue frequency with free tubulin concentration suggests that rescue occurs when a single GTP-tubulin adds onto the GDP-tubulin end of a rapidly shortening microtubule. The second order association constants, determined from the slopes of the linear regression lines in Fig. 8, are  $0.006$  and  $0.026 \mu\text{M}^{-1} \text{s}^{-1}$  for the plus and minus ends, respectively. These rates are  $\sim 1,500$  and  $165$  times smaller than the rate of GTP-tubulin addition to the GTP-tubulin ends of elongating microtubules.

From the GTP cap model, one might expect that the frequencies of seeded nucleation and rescue at each end would have the same relative dependence upon tubulin concentration since both transitions require the formation of an elongation competent microtubule end (the cap). However, our data

indicate that this is not the case, since the plus end nucleates from the axoneme more frequently (Fig. 6), while the minus end rescues more frequently (Fig. 8). Thus, seeded nucleation and rescue are not due to identical mechanisms.

### Implications for Steady State

Because of the theoretical importance of steady state, we have used the values we obtained for rate constants and transition frequencies at various tubulin concentrations to calculate a “predicted” steady state free tubulin concentration ( $S_{ss}$ ), and to compare this with the values for  $S_{ss}$  determined using centrifugation (see Materials and Methods). Interestingly, these calculations also make significant predictions regarding the phenomenon of treadmilling and length redistribution of microtubules at steady state.

We assumed for simplicity that microtubules were always rescued before complete depolymerization, did not undergo pause states, and that a linear relationship existed between tubulin concentration and the frequencies of catastrophe and rescue. Thus, at a specific tubulin concentration, the net gain of subunits at one end of a microtubule is the rate of elongation ( $v^e$ ) times the average time spent in the elongation phase ( $t^e = 1/k_c$ ), minus the rate of subunit loss during rapid shortening ( $v^{rs}$ ) times the average time spent in the rapid shortening phase ( $t^{rs} = 1/k_r$ ). Dividing by the total time of an average elongation/rapid shortening cycle ( $t^e + t^{rs}$ ), the average gain or loss of subunits per unit time is:

$$[v^e(t^e) - v^{rs}(t^{rs})]/(t^e + t^{rs}).$$

We then could sum the rates predicted at each end to determine the combined rate of gain (or loss) for an “average” microtubule for a given tubulin concentration. The results of calculations for plus end, minus end, and combined growth, presented in Fig. 9, illustrate several points.

First, our calculated value for  $S_{ss}$  agrees well with values obtained using centrifugation methods. The predicted  $S_{ss}$  corresponds to the point where the sum of the net growth for both ends of our average microtubule equals zero. From Fig. 9, this point is at  $\sim 10.9 \mu\text{M}$  tubulin. For comparison, our measurement of  $S_{ss}$  by warm centrifugation of steady state microtubules produced a value of  $6.9\text{--}7.5 \mu\text{M}$  tubulin. Thus, given the uncertainties inherent in our assumptions and measurements, the agreement of the theoretical prediction with our experimental measurements is surprisingly good.

Second, our calculations demonstrate that dynamic instability can produce a net flux of subunits through steady state microtubules, i.e., treadmilling. This is shown in Fig. 9, where, at our calculated steady state, the aggregate effects of differential elongation rates and transition frequencies predict a net subunit loss of  $\sim 13.1$  dimers  $\text{s}^{-1}$  from the plus ends of microtubules, and a net gain of about  $13.1$  dimers  $\text{s}^{-1}$  from minus ends. This correlates nicely with our observation that, although plus ends grew faster at a given concentration of tubulin, they were rescued much less often than microtubules with free minus ends. Thus, long incubations at intermediate concentrations ( $10\text{--}11 \mu\text{M}$ ) of tubulin often produced axonemes with more, and longer, microtubules at the minus end. Further, our predicted treadmilling rate is very similar to that observed for “MAP-depleted” microtubules by Farrell et al. (14) ( $16.1$  dimers  $\text{s}^{-1}$ ).

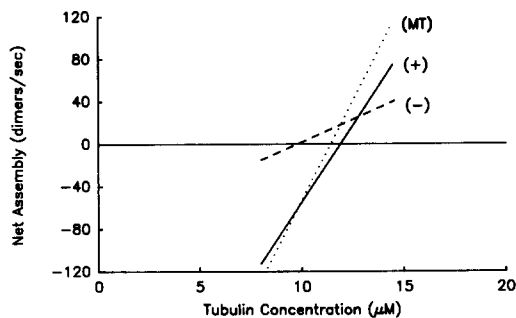


**Figure 9.** Estimated polymer dynamics at steady state. The net rate of assembly for each end was calculated (see Discussion) from the elongation rates, rapid shortening rates, and transition frequencies determined in this study. Plus end (solid line), minus end (dashed line), and the combined values (dotted line) for an “average microtubule” (MT) are plotted over the tubulin concentration range analyzed. The combined net rate of assembly was equal to zero at 10.9  $\mu\text{M}$ . At this concentration, there is net tubulin association at the minus ends and net tubulin dissociation at the plus ends.

The idea that treadmilling results from differences in the dynamic instability of opposite microtubule ends is fundamentally different from the mechanism for subunit flux through a polymer proposed by Wegner (45). Wegner showed that treadmilling required that an irreversible change take place in a subunit during binding to a polymer end. This irreversible change was thought to be hydrolysis of bound ATP for actin assembly (45) and GTP for microtubule assembly (3). Nucleotide triphosphate hydrolysis allowed the critical concentration for net assembly at opposite polymer ends to be different, resulting in net subunit flux. The Wegner model presumed that no cap of nucleotide triphosphate existed at the polymer ends, that only subunits containing nucleotide diphosphate would dissociate from the polymer, and that there was only a single phase of assembly and disassembly, during which the association of nucleotide triphosphate subunits and dissociation of nucleotide diphosphate subunits took place continuously. In contrast, instead of one continuous assembly–disassembly phase, microtubules have now been shown to exhibit alternating phases of slow elongation and rapid shortening (17, 28). Further, the present work describes a significant rate of dissociation during the elongation phase that takes place without any apparent phase transition, implying that the irreversible step (GTP hydrolysis) takes place subsequent to the association step. Therefore our results are consistent with the presence of a GTP cap, as well as the idea that GTP as well as GDP subunits can dissociate from the polymer.

If dissociation during elongation is a reversible dissociation of GTP subunits, then, as pointed out by Wegner (45), the critical concentration of each end during elongation must be equal, a result that is consistent with our observations. Thus, instead of establishing a different critical concentration for elongation at opposite microtubule ends, hydrolysis of GTP seems to allow the existence of two alternating phases of assembly and disassembly at each end of each microtubule, and also allows the frequencies of interconversion (particularly rescue) between these phases to be substantially different at opposite ends, resulting in the effect of treadmilling.

However, we should point out for completeness that, if the

GTP cap is only one subunit deep per protofilament, GTP-tubulin subunits would dissociate from GDP-tubulin subunits of opposite polarity at the two microtubule ends, allowing the critical concentrations at opposite microtubule ends to be different. If the critical concentrations were substantially different, the x-intercept of elongation rate versus tubulin concentration (Fig. 4) would be different for the two ends. Since our results show very little difference between  $S_c^e$  values for the two ends, we conclude that the effect of the GTP–GDP-tubulin boundary is minimal. Further, the possibility of different  $S_c^e$  values at opposite microtubule ends still will not allow treadmilling, as originally envisioned, to occur. If microtubules at steady state were undergoing a continuous net dissociation at one end and net association at the other, one end would quickly lose its cap and begin to rapidly disassemble.

Our data also predict that the redistribution of microtubule lengths with time, known to be a consequence of dynamic instability (23, 28), will be strongly dependent upon the initial lengths of the microtubules in the population. At 10.9  $\mu\text{M}$  free tubulin, our data show that an average rapid shortening event would involve the loss of  $\sim 12 \mu\text{m}$  at the plus end, and  $\sim 4 \mu\text{m}$  at the minus end. These values indicate that the incidence of complete microtubule loss at steady state, due to catastrophe without rescue, would decrease dramatically for microtubules much longer than 30–50  $\mu\text{m}$ . This implies that measurement of length redistribution in bulk populations ceases to be a valid indicator of dynamic instability when average microtubule lengths become  $>30\text{--}50 \mu\text{m}$ . This prediction fits nicely with the observations of Sammak et al. (35) and also with those of Farrell et al. (14), who showed that dynamic instability did not usually result in complete disassembly of microtubules that were, respectively, 20–50 and 65–75  $\mu\text{m}$  long.

Sammak et al. (35) and Farrell et al. (14) used the terms “tempered instability” and “phase dynamics,” respectively, to describe microtubule dynamics in which microtubules are almost always rescued before complete disassembly. However, our understanding of the term dynamic instability, as originally proposed by Mitchison and Kirschner (28) and described in the Introduction, includes the possibility of rescue. Further, we have shown how the parameters of dynamic instability of individual microtubules can be extended to explain the behavior of microtubule populations. Thus, like treadmilling, the special situations described by the terms tempered instability and phase dynamics can be included within the more general framework of “dynamic instability.”

### Comparisons to Dynamic Instability In Vivo

Fluorescence studies of microtubule dynamics in animal cells have shown that tubulin within the labile microtubules in the mitotic spindle exchanges with tubulin in the cellular pool with a half-time of 15–70 s, depending on species and temperature (11, 34). In the bipolar spindle of BSC1 cells at steady state, for example, the half-life of tubulin is 37 s at 31°C (42), which corresponds to a catastrophe frequency of  $(\ln 2)/37 = 0.019 \text{ s}^{-1}$ , and an average duration of elongation of  $\sim 1 \text{ min}$  (evidence indicates that rescue is not significant (29)). By using 4  $\mu\text{m}$  as the minimum estimate for average microtubule length in the BSC1 spindle, the average elongation velocity is 4  $\mu\text{m}/\text{min}$ . In our in vitro system, plus end elongation at 4  $\mu\text{m}/\text{min}$  requires an active tubulin concen-

tration of approximately 17  $\mu\text{M}$  (Fig. 4). The frequency of catastrophe in our in vitro system will be  $\sim 0.001 \text{ s}^{-1}$  at 17  $\mu\text{M}$  (Fig. 7): an order of magnitude slower than that exhibited by spindle microtubules in vivo.

In BSC1 cells at interphase, the half-life of tubulin within the labile microtubules is  $\sim 200\text{--}300 \text{ s}$  (34, 37), and the rate of microtubule elongation is about 4  $\mu\text{m}/\text{min}$  (37). The actual frequency of catastrophe for labile microtubules in the CMTC of BSC1 cells is difficult to estimate from available data, because, in contrast to the mitotic spindle, rescue appears to play a significant role in CMTC dynamics. This is indicated by the distribution of microtubule lengths at steady state (10) and the faster rate of tubulin turnover in microtubules at the cell periphery in comparison to those near the centrosome (35). For microtubules elongating at 4  $\mu\text{m}/\text{min}$  in our in vitro system, the corresponding frequency of catastrophe would be  $\sim 0.001 \text{ s}^{-1}$ , and the average microtubule length would be  $>60 \mu\text{m}$ . Since the average length of microtubules in the BSC1 interphase array is about 20  $\mu\text{m}$ , the frequency of catastrophe for the labile microtubules in the CMTC must be significantly greater than predicted from our in vitro data. In addition, because the rates of microtubule elongation in the CMTC and the mitotic spindle are similar, mitotic microtubules with an average length of 4  $\mu\text{m}$  must have an even higher frequency of catastrophe and/or lower frequency of rescue than the microtubules of the CMTC.

The above discussion indicates that we need to search for factors or conditions in the cell which promote: (a) high frequencies of catastrophe at high rates of microtubule elongation during mitosis and/or interphase; and (b) high frequencies of rescue during interphase. Possibilities include: the ionic environment (we may need to search for a buffer that matches in vivo conditions), tubulin species, tubulin modifications, and MAPs. Modulation of such factors and/or conditions probably controls the dynamics of the labile microtubules in the spindle and the CMTC, and may regulate the rapid shifts in mean microtubule length and mean life-time that occur during the transitions between the interphase and the mitotic phases of the cell cycle.

Lynne Cassimeris provided advice and participated in many helpful discussions. Dr. Michael Caplow provided continuous discussion and numerous insights. We are grateful to Drs. Albert Harris and Bruce Nicklas for generous loans of equipment, and to Dr. Elizabeth Harris for the gift of *Chlamydomonas*. E. D. Salmon wishes to thank Neal Glikzman and Shinya Inoué for stimulating discussions. Cate Parker, Susan Whitfield, and Vicki Petrie provided excellent illustrations and photographs. Brenda Bourns assisted in data collection and analysis, and aided in the preparation of the manuscript. Finally, we are indebted to Bill Sims, who aided in the construction of the image processing system.

This work was supported by National Institute of Health grants GM24364 to E. D. Salmon and GM28553 to H. P. Erickson.

Received for publication 25 February 1988, and in revised form 20 June 1988.

## References

- Allen, R. D., N. S. Allen, and J. L. Travis. 1981. Video-enhanced differential interference contrast (AVEC-DIC) microscopy: a new method capable of analyzing microtubule-related movement in the reticulopodia of *Allogromia laticollaris*. *Cell Motil.* 1:191-302.
- Bell, C. W., C. Fraser, W. S. Sale, W.-J. Y. Tang, and I. R. Gibbons. 1982. Preparation and purification of dynein. *Methods Cell Biol.* 24:373-397.
- Bergen, L. G., and G. G. Borisy. 1980. Head-to-tail polymerization of microtubules in vitro: an electron microscopic analysis of seeded assembly. *J. Cell Biol.* 84:141-150.
- Bergen, L. G., and G. G. Borisy. 1982. A direct method for analyzing the polymerization kinetics at the two ends of a microtubule. *Methods Cell Biol.* 24:171-187.
- Caplow, M. 1986. Location of the guanosine triphosphate (GTP) hydrolysis site in microtubules. *Ann. NY Acad. Sci.* 466:510-518.
- Caplow, M., and R. Reid. 1985. Directed elongation model for microtubule GTP hydrolysis. *Proc. Natl. Acad. Sci. USA.* 82:3267-3276.
- Carlier, M.-F., and D. Pantaloni. 1981. Kinetic analysis of guanosine 5'-triphosphate hydrolysis associated with tubulin polymerization. *Biochemistry.* 20:1918-1924.
- Carlier, M.-F., D. Didry, and D. Pantaloni. 1987. Microtubule elongation and guanosine 5'-triphosphate hydrolysis. Role of guanine nucleotides in microtubule dynamics. *Biochemistry.* 26:4428-4437.
- Carlier, M.-F., T. L. Hill, and Y.-D. Chen. 1984. Interference of GTP hydrolysis in the mechanism of microtubule assembly: an experimental study. *Proc. Natl. Acad. Sci. USA.* 81:771-775.
- Cassimeris, L. U., P. Wadsworth, and E. D. Salmon. 1986. Dynamics of microtubule depolymerization in monocytes. *J. Cell Biol.* 102:2023-2032.
- Cassimeris, L. U., R. A. Walker, N. K. Pryer, and E. D. Salmon. 1987. Dynamic instability of microtubules. *Bioessays.* 7:149-154.
- Chen, Y., and T. L. Hill. 1985. Monte Carlo study of the GTP cap in a five-start helix model of a microtubule. *Proc. Natl. Acad. Sci. USA.* 82:1131-1135.
- David-Pfeuty, T., H. P. Erickson, and D. Pantaloni. 1977. Guanosinetriphosphatase activity of tubulin associated with microtubule assembly. *Proc. Natl. Acad. Sci. USA.* 74:5372-5376.
- Farrell, K. W., M. A. Jordan, H. P. Miller, and L. Wilson. 1987. Phase dynamics at microtubule ends: the coexistence of microtubule length changes and treadmilling. *J. Cell Biol.* 104:1035-1046.
- Gard, D. L., and M. W. Kirschner. 1987. A microtubule-associated protein from *Xenopus* eggs that specifically promotes assembly at the plus end. *J. Cell Biol.* 105:2203-2215.
- Hill, T. L., and Y. Chen. 1984. Phase changes at the end of a microtubule with a GTP cap. *Proc. Natl. Acad. Sci. USA.* 81:5772-5776.
- Horio, T., and H. Hotani. 1986. Visualization of the dynamic instability of individual microtubules by dark-field microscopy. *Nature (Lond.).* 321:605-607.
- Inoué, S. 1981. Video image processing greatly enhances contrast, quality, and speed in polarization-based microscopy. *J. Cell Biol.* 89:346-356.
- Johnson, K. A., and G. G. Borisy. 1977. Kinetic analysis of microtubule assembly in vitro. *J. Mol. Biol.* 117:1-31.
- Karr, T. L., A. E. Podrasky, and D. L. Purich. 1979. Participation of guanine nucleotides in nucleation and elongation steps of microtubule assembly. *Proc. Natl. Acad. Sci. USA.* 76:5475-5479.
- Kirschner, M. W., and T. Mitchison. 1986. Microtubule dynamics. *Nature (Lond.).* 324:621.
- Kobayashi, T. 1975. Dephosphorylation of tubulin-bound guanosine triphosphate during microtubule assembly. *J. Biochem. (Tokyo).* 77:1193-1197.
- Kristofferson, D., T. Mitchison, and M. Kirschner. 1986. Direct observation of steady-state microtubule dynamics. *J. Cell Biol.* 102:1107-1019.
- Leslie, R. J., W. M. Saxton, T. J. Mitchison, B. Neighbors, E. D. Salmon, and J. R. McIntosh. 1984. Assembly properties of fluorescein-labeled tubulin in vitro before and after fluorescence bleaching. *J. Cell Biol.* 99:2146-2156.
- Lutz, D. A., and S. Inoué. 1986. Techniques for observing living gametes and embryos. *Methods Cell Biol.* 27:89-110.
- Merril, C. R., D. Goldman, S. A. Sedman, and M. H. Ebert. 1981. Ultrasensitive stain for proteins in polyacrylamide gels shows regional variation in cerebrospinal fluid proteins. *Science (Wash. DC).* 211:1437-1438.
- Mitchison, T., and M. Kirschner. 1984. Microtubule assembly nucleated by isolated centrosomes. *Nature (Lond.).* 312:232-237.
- Mitchison, T., and M. Kirschner. 1984. Dynamic instability of microtubule growth. *Nature (Lond.).* 312:237-242.
- Mitchison, T., L. Evans, E. Schulze, and M. Kirschner. 1986. Sites of microtubule assembly and disassembly in the mitotic spindle. *Cell.* 45:515-527.
- Morrisey, J. H. 1981. Silver stain for proteins in polyacrylamide gels: a modified procedure with enhanced sensitivity. *Anal. Biochem.* 117:307-310.
- O'Brien, E. T., W. A. Voter, and H. P. Erickson. 1987. GTP hydrolysis during microtubule assembly. *Biochemistry.* 26:4148-4156.
- Penningroth, S. M., and M. Kirschner. 1977. Nucleotide binding and phosphorylation in microtubule assembly in vitro. *J. Mol. Biol.* 115:643-673.
- Pryer, N. K., P. Wadsworth, and E. D. Salmon. 1986. Polarized microtubule gliding and particle saltations produced by soluble factors from sea urchin eggs and embryos. *Cell Motil.* 6:537-548.
- Salmon, E. D., and P. Wadsworth. 1986. Fluorescence studies of tubulin and microtubule dynamics in living cells. In *Applications of Fluorescence in the Biomedical Sciences*. D. L. Taylor, A. S. Waggoner, R. F. Murphy, F. Lanni, and R. R. Birge, editors. Alan R. Liss, Inc., New York.

- 377-403.
35. Sammak, P. J., G. J. Gorbsky, and G. G. Borisy. 1987. Microtubule dynamics in vivo: a test of mechanisms of turnover. *J. Cell Biol.* 104:395-405.
  36. Schnapp, B. J. 1986. Viewing single microtubules by video light microscopy. *Methods Enzymol.* 134:561-573.
  37. Schulze, E., and M. Kirschner. 1986. Microtubule dynamics in interphase cells. *J. Cell Biol.* 102:1020-1031.
  38. Taylor, J. R. 1982. *An Introduction to Error Analysis.* University Science Books, Mill Valley, CA. 207-217.
  39. Voter, W. A., and H. P. Erickson. 1982. Electron microscopy of MAP 2. *J. Ultrastruct. Res.* 80:374-382.
  40. Voter, W. A., and H. P. Erickson. 1984. the kinetics of microtubule assembly. *J. Biol. Chem.* 259:10430-10438.
  41. Voter, W. A., E. T. O'Brien, and H. P. Erickson. 1987. A calculation of the GTP cap size based on observed frequencies of microtubule catastrophe. *Biophys. J.* 51:214a. (Abstr.)
  42. Wadsworth, P., and E. D. Salmon. 1986. Analysis of the treadmilling model during metaphase of mitosis using fluorescence redistribution after photobleaching. *J. Cell Biol.* 102:1032-1038.
  43. Wadsworth, P., and E. D. Salmon. 1986. Preparation of fluorescent tubulin. *Methods Enzymol.* 134:519-528.
  44. Deleted in proof.
  45. Wegner, A. 1976. Head-to-tail polymerization of actin. *J. Mol. Biol.* 108:139-150.
  46. Weisenberg, R. C., W. J. Deery, and P. J. Dickinson. 1976. Tubulin-nucleotide interactions during polymerization and depolymerization of microtubules. *Biochemistry.* 15:4248-4254.
  47. Yanagisawa, T., S. Hasegawa, and H. Mohri. 1968. The bound nucleotides of the isolated microtubules of sea urchin sperm flagella and their possible role in flagellar movement. *Exp. Cell Res.* 52:86-100.
  48. Zeeberg, B., and M. Caplow. 1981. An isoenergetic exchange mechanism which accounts for tubulin-GDP stabilization of microtubules. *J. Biol. Chem.* 256:12051-12057.